LA-UR-99-147

Effect of the Plutonium α–β Phase Transition Expansion on Storage Can Integrity

Dane R. Spearing, NMT-6
D. Kirk Veirs, NMT-6
F Coyne Prenger, ESA-EPE

January 14, 1999

Los Alamos
National Laboratory

Los Alamos National Laboratory is operated by the University of California for the United States Department of Energy under contract W-7405-ENG-36.

This work was supported by the Nuclear Materials Stewardship Project Office of the US Department of Energy.

An Affirmative Action/Equal Opportunity Employer

Effect of the Plutonium $\alpha-\beta$ Phase Transition Expansion on Storage Can Integrity

Dane R. Spearing[†], D. Kirk Veirs[†], and F. Coyne Prenger[*]

[†]Nuclear Materials Technology Division
[*]Engineering Sciences & Applications Division
Los Alamos National Laboratory
Los Alamos, NM 87545

ABSTRACT

This study was performed to experimentally determine the effects of the volume expansion of plutonium metal undergoing the alpha to beta phase transition on a stainless steel storage container of the type specified by the Department of Energy plutonium storage standard (DOE, 1996). A monolithinc cylindrical plutonium ingot was placed in the axial center of an annealed stainless steel cylinder with an inner diameter 0.004” larger than the outer diameter of the ingot. The geometry maximizes the strength of the plutonium ingot with respect to the confining stainless steel cylinder and represents a “worst case” geometry for assessing the possibility of containment failure. The ingot was thermally cycled until equilibrium in the strain response was reached at six cycles. Based the experimental results detailed herein, the total strain that was imparted to the stainless steel cylinder through six thermal cycles was 2.03% and expansion of the ingot in the axial direction was measured to be greater than 5%, as compared to 3% for each direction expected for isotropic expansion. Elastic strain was measured to be ~0.2%, which implies that the maximum radial pressure that the cylinder imparts upon the Pu ingot is 1,300 psi. This is an order of magnitude less than the compressive yield strength for both α-Pu (~60,000 psi) and β-Pu (~20,000 psi) at the transition temperature. This enhanced anisotriopic expansion is attributed to preferentially oriented grain growth of the β-Pu along the axial direction (perpendicular to the stress applied by the steel cylinder).

INTRODUCTION

The current US Department of Energy (DOE) standard for the stabilization, packaging, and storage of plutonium bearing materials (DOE, 1996) specifies a maximum temperature of 100°C for the storage of alpha-phase Pu metal (α-Pu). The rational for this maximum temperature was to prevent the possibility of compromising the integrity of the standard-specified stainless steel storage cans due to the large volume expansion (~10%) associated with the plutonium alpha to beta phase transition, which occurs at ~120°C. The assumption was that pieces of α-Pu metal tightly fit within the container had the potential for deforming the wall of a storage container beyond accepted criteria (ASME, 1995) upon transforming to β-Pu and/or via repeated cycling through the α/β transition. Within current proposed storage facilities (such as the Actinide Storage Facility at the Savannah River Site), credible scenarios exist in which local temperatures could significantly exceed the Pu α/β transition temperature. (As an example, the cooling system could fail and self-heating and insulating conditions could raise the plutonium metal temperature above 120°C). Thus, the purpose of this study was to experimentally determine the effects of the volume expansion of the alpha to beta transformation of plutonium metal on a stainless steel storage container of the type specified by the plutonium storage standard.

LITERATURE REVIEW

A number of studies have been published on the effects of a variety of variables (e.g. - pressure, deformation, grain size) relevant to the Pu α–β phase transition, which can be used to make qualitative predictions as to how the Pu and storage container will interact though the course of thermal cycling through the phase transition. The mechanism of the α–β phase transition is still not well understood, although several studies suggest that it is martensitic in nature (Nelson and Shyne, 1966a; Nelson and Shyne, 1966b). The α to β and β to α transformation kinetics have been extensively studied, and show that the transformations occur isothermally and exhibit simple TTT curves with significant hysteresis between the β to α and α to β (Nelson and Shyne, 1966b; Rechtien and Nelson, 1973). The effects of deformation and stress on the kinetics of the phase

transition have also been examined (Nelson and Shyne, 1966a; Rechtien and Nelson, 1973), and it was found that plastic deformation of the α-phase accelerates the α to β transformation, with the acceleration attributable only to residual stresses. It was also found that plastic deformation of the β-phase retards kinetics of the back transformation from β to α. Thus, plastic deformation tends to stabilize the higher temperature β-phase. Conversely, Nelson and Shyne (1966a) found that applied uniaxial compressive stress raises the starting temperatures for both the α to β and β to α transformations, while tensile stress lowered the α to β starting temperature. This is consistent with the experimentally determined P-T phase diagram for pure plutonium (Stephens, 1963), in which the α–phase is stabilized by increasing isostatic pressure.

The effect of applied stress on grain orientation and grain growth has been studied, and it was found that α-Pu displays a preferential growth in specific crystallographic directions as a function of the applied distribution of elastic stresses during the β to α phase transition (Spriet, 1965). This technique has in fact been used to grow oriented specimens of Pu for electrical resistivity studies (Elliot et al., 1964). Interestingly, Nelson and Shyne (1966a) observed that, in the absence of any applied stresses, both the α to β and β to α transformation volume changes occur anisotropically. Based on this observation, they conclude that these anisotropic transformation strains imply that there must be a specific crystallographic orientation relationship between the α and β phases with respect to the phase transition.

Lastly, it is well established that transformation damage in the form of microcracks and voids is induced upon thermal cycling through the α–β transition. Nelson (1966) found that the size and number of cracks increased with continued α–β cycling, which led to a volume expansion of the Pu metal specimens of as much as 3% (0.6 g/cc) per cycle. A number of factors were found to influence the presence and pervasiveness of this transformation-induced damage, including how the parent β-phase was formed, concentration of impurities, transformation temperature, heating/cooling rates, and applied stresses.

Based on the aforementioned available literature and previous studies, there are obviously a large number of variables which could influence how constrained pieces of α-Pu metal within a

stainless steel storage container might behave when cycled through the α/β phase transition, and what effect the Pu metal may have on the integrity of the container. This illustrates the necessity for experimentally determining what effects the volume expansion associated with the α/β phase transition of plutonium metal may have on the integrity of such a container.

PREVIOUS EXPERIMENT

A previous study was conducted at Los Alamos National Laboratory in 1997 to address the issues of storage can integrity (Flamm et al., 1997). The results from this study are summarized below.

In the previous experiment, a 4.4 kg cast cylindrical ingot of α-Pu metal, measuring 11.3 cm in diameter and 2.13 cm in thickness with a density of 19.4 g/cc, was inserted, as cast, into a drawn stainless steel container of the type used for the LANL ARIES (Advanced Recovery and Integrated Extraction System) project. There was approximately a 0.025 in. gap between the Pu ingot and the inside of the container. The Pu ingot was placed on a copper disk stand-off on the bottom of the container, and strain gauges were placed on the outside of the container around the circumference at the height of the Pu ingot to measure induced strain in the container (see Figure 1). This assembly was then heated on a hot-plate and repeatedly cycled through the Pu α/β phase transition while the strain gauge outputs and temperature were recorded as a function of time.

After 25 cycles through the α/β phase transition, the results of this experiment are that a total of 0.005 in. of radial deformation was imparted on the stainless steel storage canister, corresponding to approximately 0.2% plastic strain. The maximum amount of plastic strain was reached at 5 cycles, after which no additional plastic strain was accumulated. The maximum total strain observed was approximately 0.7% (0.5% elastic strain + 0.2% plastic). In addition, after the first cycle, the Pu ingot was found to have increased in thickness by approximately 10%.

It was calculated that the amount of constraining pressure put on the Pu ingot during the elastic deformation of the can was about 3500 psi, which is well below both the compressive yield strengths of α-Pu (~60,000 psi) and β-Pu (~20,000 psi) at the transition temperature (Gardner,

1980). Based on the experimental results summarized above, and the calculated constraining pressure on the Pu ingot, it was concluded from this experiment that the Pu ingot itself deformed during the phase transition at pressures far below its compressive yield strength, most likely due to preferential grain orientation of the Pu during the α–β phase transition. Furthermore, the total amount of strain (plastic and elastic) induced in the stainless steel storage container (0.7%) was far below what is necessary for containment failure.

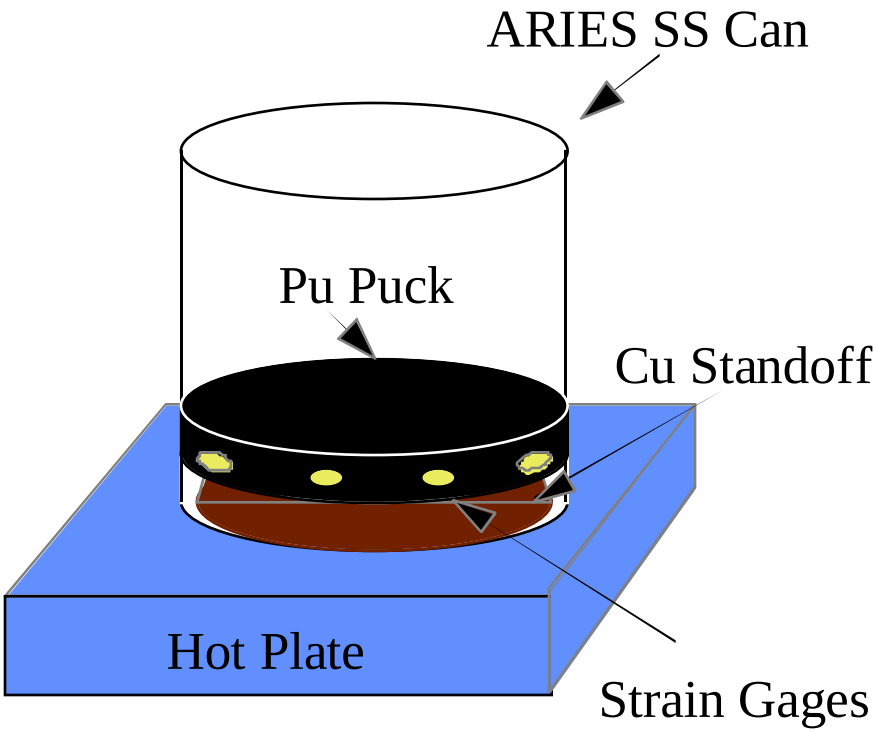

Fig 1 – Schematic of previous experimental setup (Flamm et al, 1997)

EXPERIMENT RATIONALE

A second experiment was deemed necessary for several reasons. Firstly, the container that was used in the previous experiment was manufactured by cold forming 316 stainless steel around a mandrel, which results in a measured yield strength of the cylinder walls of 142,000 psi. In contrast, storage containers can be manufactured such that the yield strength of the cylinder walls is ~40,000 psi, the yield strength of annealed 316 stainless steel. Secondly, the geometry of the

previous experiment made modeling of the results using finite element analysis complex due to the additional strength added by the container bottom. In addition, the use of a hot-plate as the heating source resulted in a non-uniform heating geometry. It was also determined that in-situ, real time measurements of the change in thickness of the Pu ingot would be useful in assessing the effect of the constraining pressure on the ingot geometry during the phase transition. Lastly, a near zero-tolerance fit between the ingot and inside of the container was desired so that the ingot was in contact with the container wall throughout the phase transition. For these reasons, a second experiment was undertaken.

EXPERIMENTAL PROCEDURE

The Pu source material used for this experiment was supplied by Savannah River, and consists of high-purity alpha phase metal with an average total impurity content of 432 ppm (exclusive of Am), and an average isotopic concentration of 93.83% ^{239}Pu. Based on the starting ^{241}Pu concentration and the age of the material, the total Americium concentration was calculated to be about 1500 ppm. The material was melted and chill cast at the plutonium foundry at Los Alamos National Laboratory into a graphite mold, which resulted in an as-cast cylindrical ingot 4.51” in diameter and 0.78” in height, with a mass of 4231.3 g. Following casting, the ingot was machined to a right circular cylinder of the following dimensions: 4.358” diameter, 0.751” thickness, 3591.7 g mass (Figure 2). Using an immersion method, the density was measured to be 19.57 g/cc. The high measured density (theoretical max. $\rho_{\alpha-Pu}$= 19.86 g/cc) and surface uniformity of the cast ingot indicated the absence of any significant microcracking or void space formation from the casting process. Previous studies indicate that the presence of certain impurities, such as Am, on the order of 1000 ppm, drastically reduce microcrack formation during casting (Nelson, 1966). Thus, the 1500 ppm Am content of the material used in this study may in part be responsible for the observed high density and lack of significant microcracking.

In order to simplify subsequent finite element analyses of the experimental results, which are being conducted by Savannah River, and eliminate any contribution to the wall strength of the

container by a bottom or lid, a steel cylinder was used to simulate a DOE standard 3013 inner canister. Several of these cylinders were manufactured at the Savannah River Site (SRS) using 316 stainless steel via a process which resulted in a fully annealed product (no remnant work hardening of the steel). The cylinders were then machined to right circular cylinders. The cylinder used for this experiment was designated as SRS Part #3, and had dimensions reported by SRS as the following: 4.359” internal diameter (ID), 4.486” outer diameter (OD), 6.008” length, 0.060” thickness. The ID was re-measured upon arrival at LANL as 4.362”, which leaves a 0.002” radial clearance between the Pu ingot and ID of the cylinder.

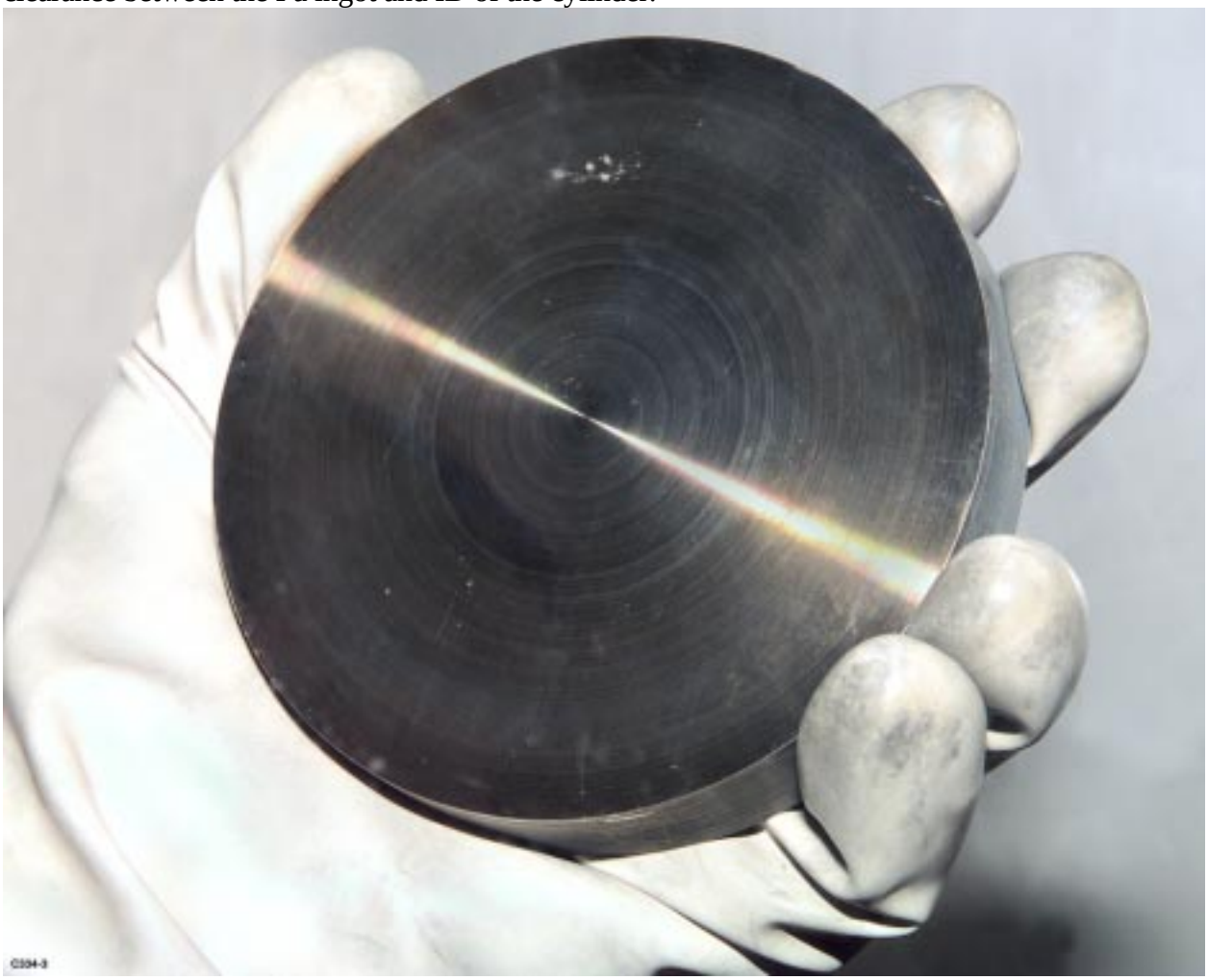

Fig 2 – Machined _-Pu ingot (4.358” diameter, 0.751” thick).

Twelve strain gages, the locations of which are shown in Figure 3, were installed on the outer surface of the cylinder as per the manufacturer’s (Micro-Measurements Division, Measurements

Group, Inc., Raleigh, NC) instructions. (All strain gage related parts listed below are from this manufacturer.) The cylinder exterior was first cleaned with ethanol to remove oils or other organics followed by dry abrading with 320 grit emory cloth. The surface was then cleaned with M-Prep Conditioner A (a phosporic acid based cleaning agent) while abrading with 320 grit emory cloth. The abraded material was removed with cotton swabs soaked in M-Prep Conditioner A. A wipe was then used to remove any liquid resulting in a dry surface. The acid on the surface was neutralized using M-Prep Neutralizer 5A (an ammonia based neutralizer).

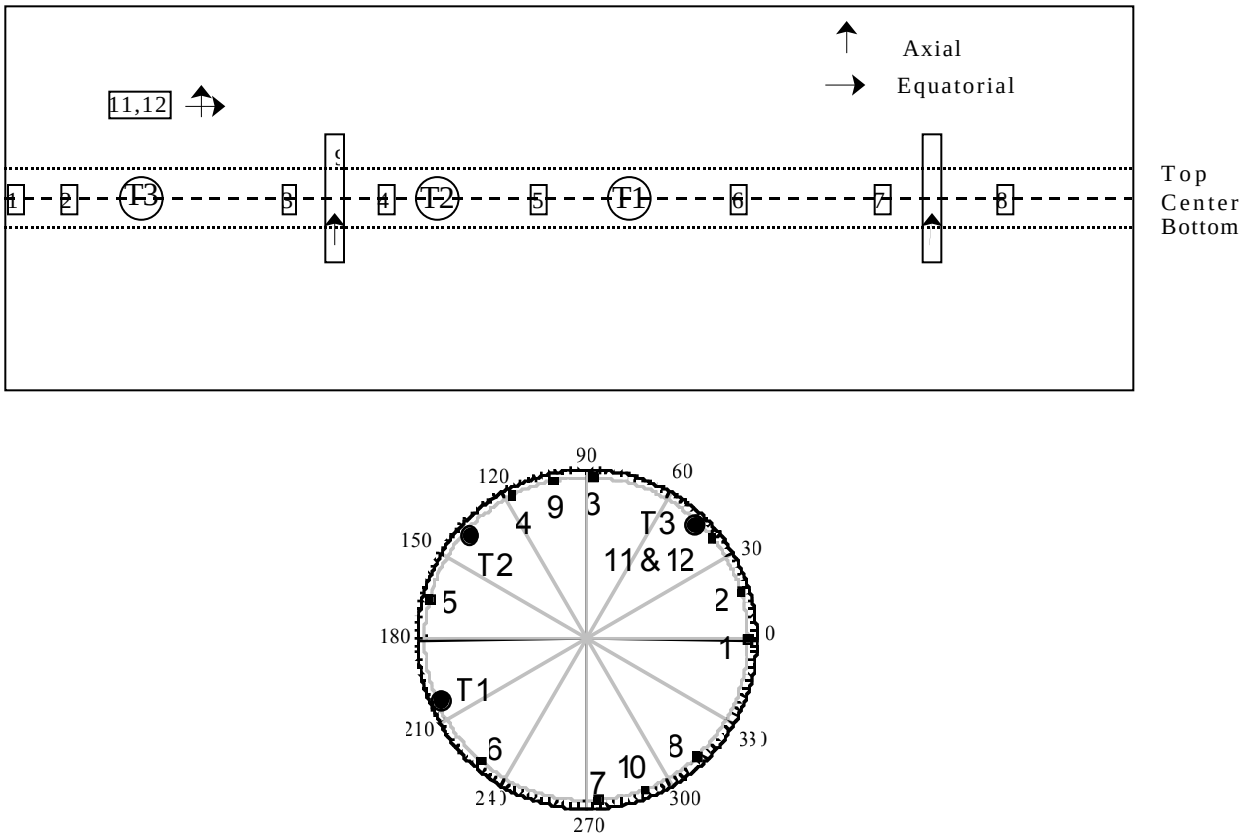

Fig 3 – Strain gage and thermocouple locations.
Top – cylinder unwrapped. *Bottom* – polar plot.
Squares – strain gage locations. *Circles* – thermocouple locations. Gages 1-8 are oriented to measure strain in the equatorial direction.

Three types of strain gages were used. Small single direction gages (part EP-08-062-DN-350) were chosen to measure the equatorial strain at the position on the tube corresponding to the axial middle of the puck. Two inch long single direction gages (part EA-06-20CRW-120) were chosen

to measure the axial strain across the entire height of the puck. A two-element 90 degree rosette was chosen to measure the axial and equatorial strains in a region on the tube far from the puck.

The first eight gages were aligned to obtain equatorial strain along the center line of the puck, gages 9 and 10 were aligned to obtain axial strain across the puck, and gages 11 and 12 were aligned to obtain axial and equatorial strain away from the puck (height of center of gage at 115 mm). The gages were bonded to the stainless steel using M-Bond 600, an epoxy good to 370 °C. The epoxy was cured at 75 °C for at least 12 hours. A Type C solder pad was used with each gage, the pads being connected to the gage via a single strain-relieved wire. The solder pads were then connected to the instrumentation using a three conductor, 30 gauge twisted cable with etched Teflon insulation rated to 260 °C (330-FTE). The solder used was a 63% tin/36.65% lead/0.35% antimony solder, which is good to 183 °C (361A-20R). The three wire configuration was used to prevent thermal drift due to resistance changes in the leads as the temperature changes. The open faced gages (EP-08-062-DN-350 and EA-06-20CRW-120) were coated with the adhesive to protect the gage during installation. After installation, all gages were coated with a silicon rubber environmental coating (M-Coat C), rated to 290 °C. The continuity of the wiring was checked after installation, and it was found that gages 2 and 4 could not be used due to bad installation; gage 2 had an open circuit and gage 4 was visibly damaged during installation.

Three K-type thermocouples (Model SA1-K, Omega, Inc.) were placed on the outside of the can in positions illustrated in Figure 2. A fourth thermocouple was placed on the Pu ingot itself during the experiment. The thermocouples were attached via self-adhesive pads which are certified for use up to 160°C. Prior to use, the thermocouples were calibrated in a controlled environment between 0° - 160°C using equipment traceable to national standards by the LANL Standards and Calibration Laboratory, and certified to be accurate to ±0.3°C. Output leads from the strain gages and thermocouples were connected to a National Instruments SCXI-1321Terminal Block. Strain and temperature data recorded at 15 second intervals during the experiment via a custom written LabView software application.

The furnace used was a Lindberg MK-6015-S, 208V 4000W horizontal open-ended tube furnace, 15” long, 6” ID with a custom built temperature controller. For all thermal cycles, heating was done from ambient temperature to 130°C at 2°C/min. Cooling was done by turning off the furnace power and letting the experiment cool to ambient. All experiments took place within an Ar-atmosphere glovebox, with O_2 levels maintained at 30 ppm or less.

Following installation of the furnace and steel cylinder into the glovebox, several strips of fiberglass cloth were laid down inside the bottom half of the tube furnace on which the cylinder was placed. This prevented direct contact of the outside of the cylinder, as well as the strain gages and thermocouples, with the heating elements of the furnace.

Fig 4 – Close up of dilatometry set up. Note quartz rod attached to dial indicator.

Thickness changes in the Pu ingot were measured using two quartz glass rod dilatometers attached to dial indicators (Part #196B, Starrett Co.), accurate to ±0.001". Readings from the dial indicators were recorded manually throughout the course of the experiments. One of the dilatometers is shown in Figure 4 and a schematic of the entire experimental setup is given in Figure 5.

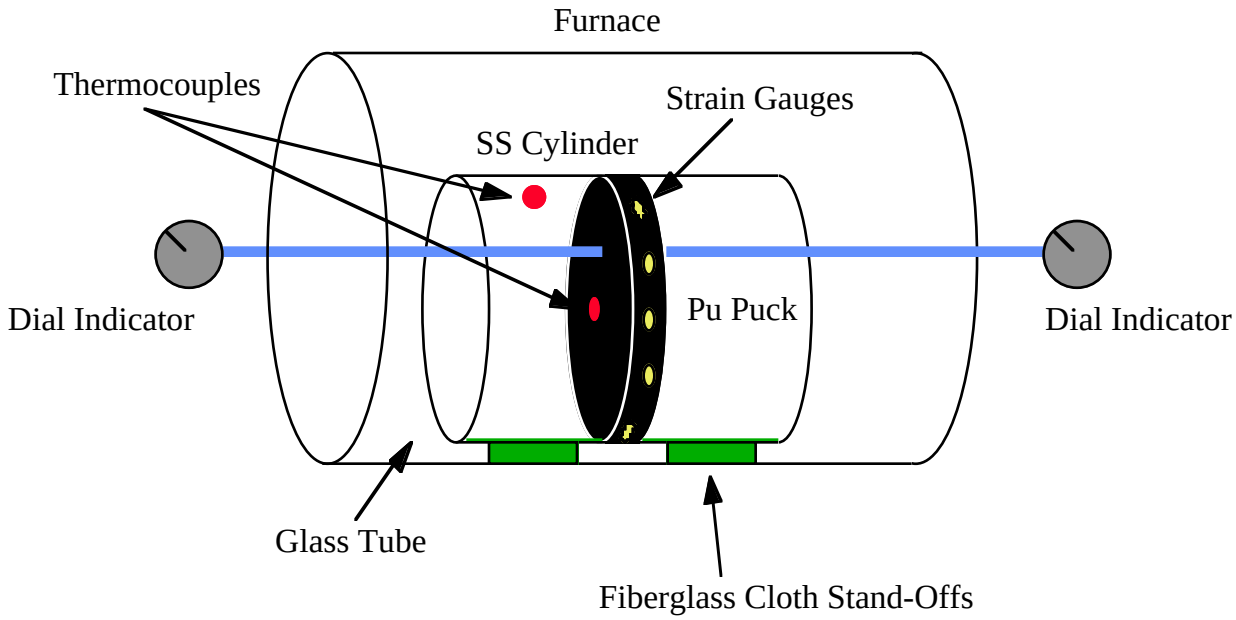

Fig 5 – Schematic of current experimental set up. Not to scale.

Prior to performing the experiment using the Pu ingot, a "dry run" was done in order to quantify the thermal response behavior of the strain gages. A brass ingot, of the same dimensions as the Pu ingot, was slid into the steel cylinder and centered by hand to act as a thermal mass. The cylinder and brass ingot were then thermally cycled in a manner identical to which the Pu ingot would be cycled (2°C/min heating rate to 150°C, 30-90 minutes at 150°C, followed by power-off cooling to ambient temperature) and the response of the strain gages recorded as a function of time and temperature. Note that no additional strains were applied to the cylinder by the brass ingot, which was used solely as a thermal mass. Results are plotted in Figure 6. The far-field and axial strain gages (9,10,11,12) showed a positive strain in response to temperature of 550±20

microstrain (με) from ambient to 130°C. The hoop strain gages showed negative strain in response to temperature of –250±20με from ambient to 130°C except for strain gage #1 which showed –170±20με.

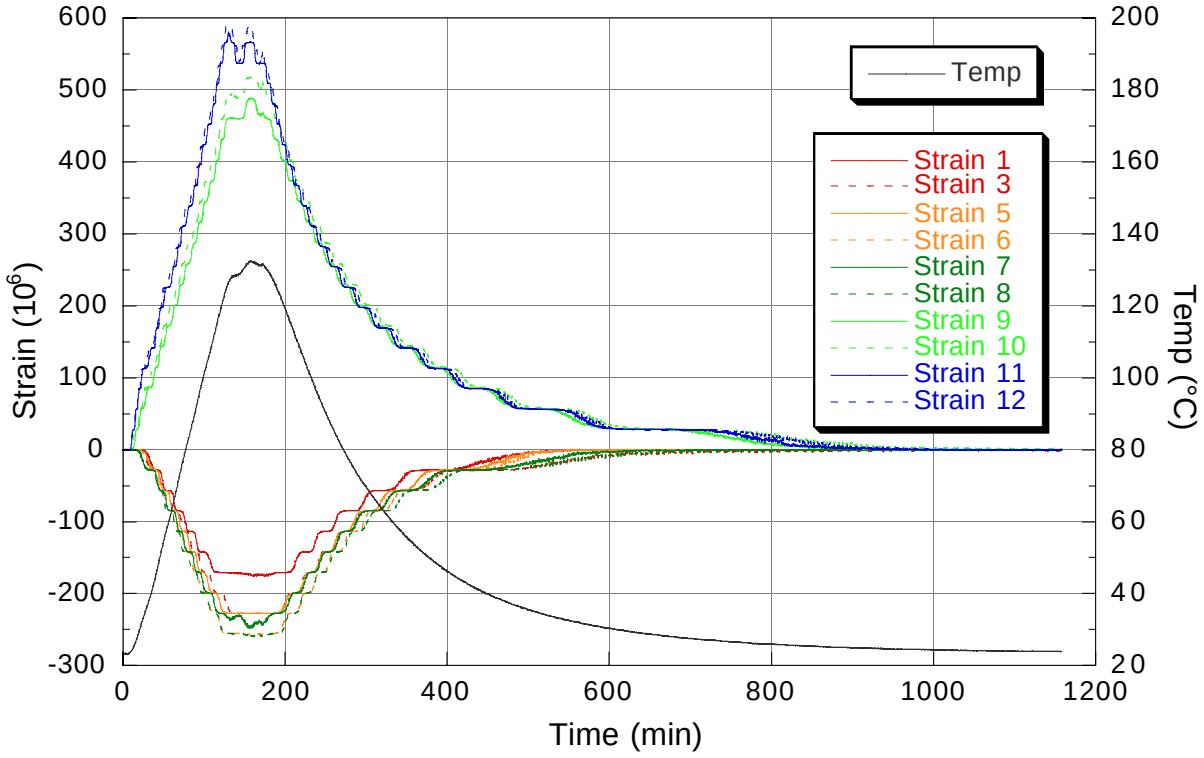

FIG 6

Strain/Temp vs. Time. Strain gage thermal with brass ingot. 30με steps are instrument resolution.

Following the dry run, the brass ingot was removed from the cylinder and the Pu ingot was inserted by hand (see Figure 7), a thermocouple was attached to the ingot, and the ingot was centered within cylinder with the aid of a ruler to within ±1 mm. The cylinder was oriented in the furnace with thermocouple T1 at the bottom, and thermocouple T3 and the far-field strain gages (11,12) at the top. Quartz glass rod dilatometers were then placed on the opposing faces of the ingot and zeroed. All strain gages were zeroed prior to the first thermal cycle. This is the only time the strain gages were zeroed so that the cumulative effects of strain as a function of cycle could be measured.

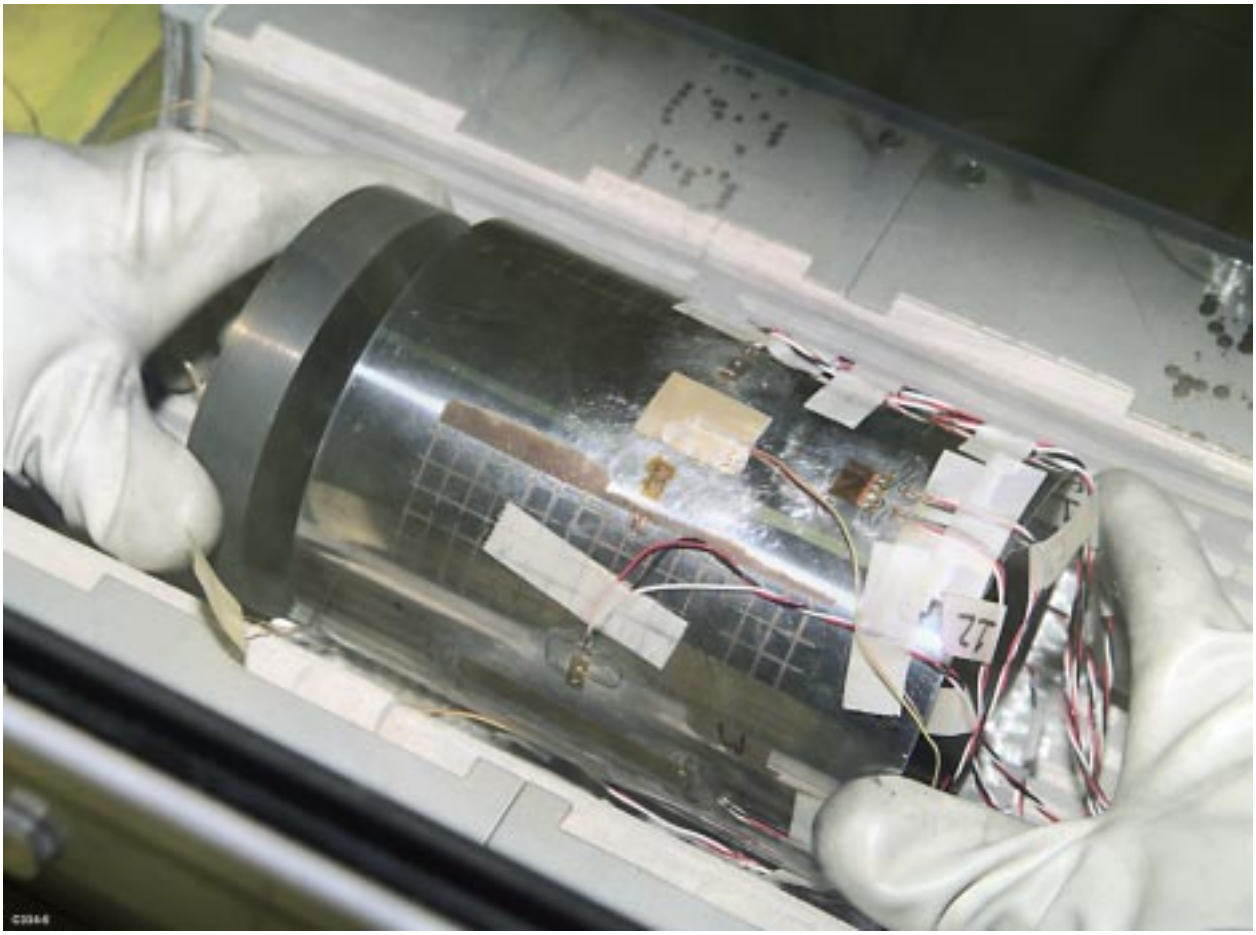

Fig 7 – Insertion of Pu ingot into stainless steel cylinder. Note strain gages and thermocouples on outside of cylinder.

RESULTS

The strain and temperature vs. time data from the first cycle are given in Figure 8. All of the hoop strain gages (1,3,5,6,7,8) showed peak positive strains ranging from 10,363με to 17,519με during the course of the thermal cycle. In contrast, the longitudinal gages (9,10) showed a slight negative strain of –2450με. The far-field gages (11,12) showed only the expected thermal response of the empty cylinder, indicating no additional strain was accumulated away from the area in which the ingot was in contact with the cylinder. (Note that the temperature plotted in Figure 8 is the temperature of the Pu ingot. Thus, the starting temperature is 52°C due to self-heating effects.) A plot of strain as a function of ingot temperature during the heating phase of the cycle is given in

Figure 9. Based on this first cycle, the calculated total strain on the steel cylinder averaged among all hoop strain gages is 1.44%. As is evident from Figure 8, a large proportion of this strain is plastic (1.27% average), given that only a small amount of strain relaxation is observed after cooling. Subtracting the plastic from the total strain leaves the elastic strain, which is 0.17% on average for the first cycle.

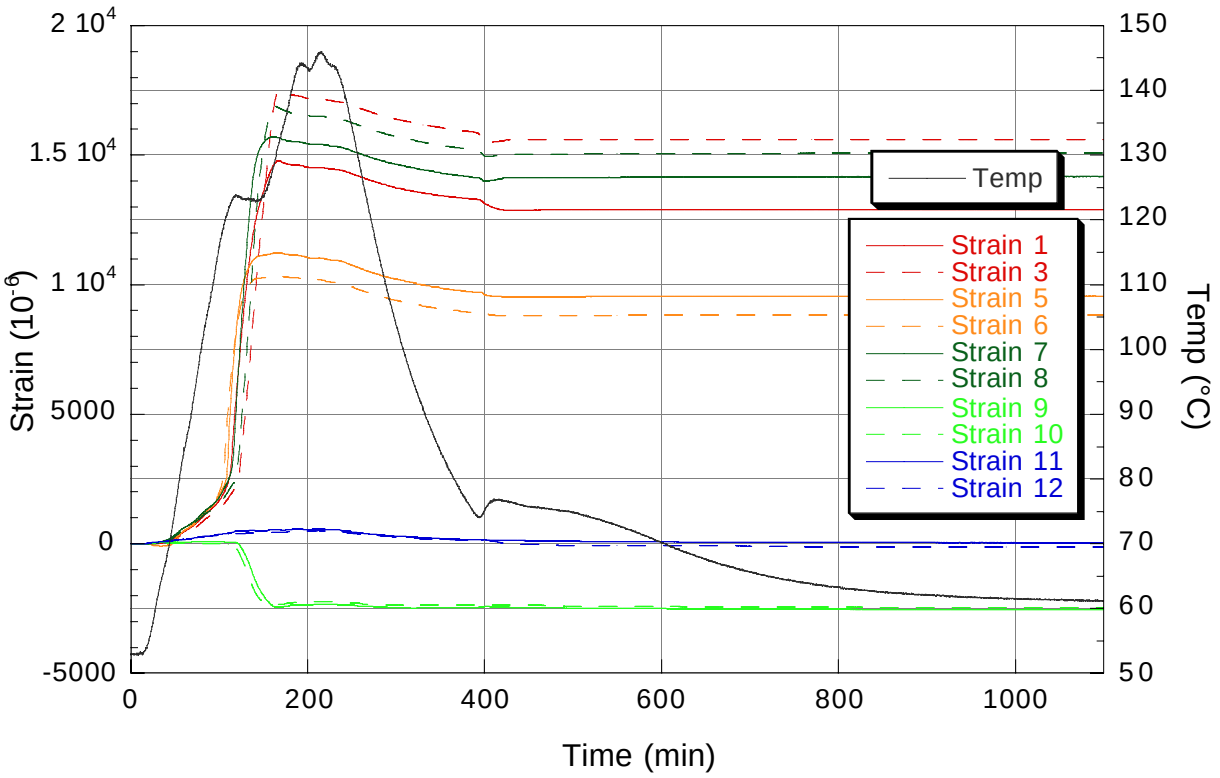

FIG 8

Strain/Temp vs. Time for first thermal cycle of Pu ingot.

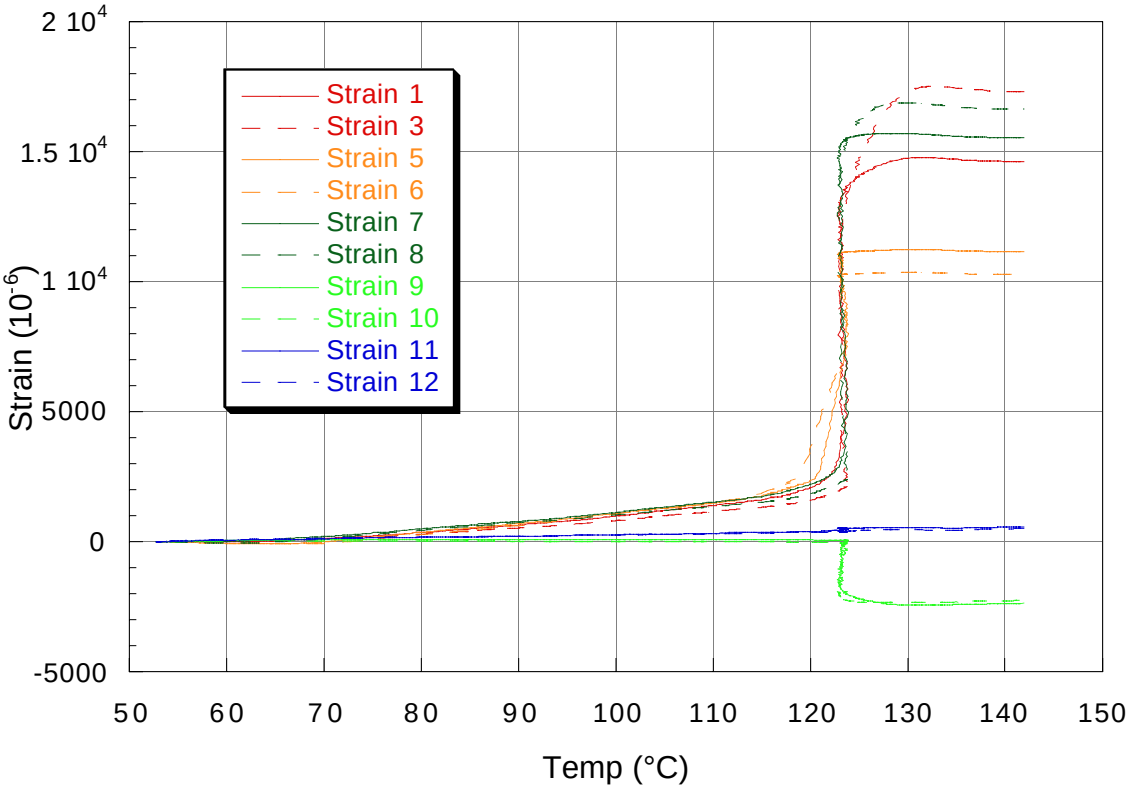

FIG 9

Strain vs. Temp for first thermal cycle of Pu ingot.

For all thermal cycles, strain gage #3 consistently showed the highest strain levels. Thus, rather than plot the output from all strain gages for all subsequent cycles, only the output from strain gage #3 will be plotted, which illustrates the maximum observed strain. A plot of strain vs. time for all six cycles for strain gage #3 is given in Figure 10. Six regimes of the strain vs. time plot for the first cycle are identified and interpreted as follows: (1) the first regime labeled represents strain accumulated due to the thermal expansion of α-Pu. Prior to this point, the flat part of the curve represents the time before the furnace was turned on, and the small amount of expansion of the α-Pu needed to close the 0.002" radial gap between the ingot and inside of the cylinder. (2) At about 120 minutes into the run, the slope of the strain vs. time curve increases, and the second region represents strain accumulation due to expansion associated with the α to β phase transition. Essentially all of the thermal energy is consumed by the endothermic α to β phase

transition, and thus the temperature does not increase significantly during this time, as can be seen in Figure 8. This is characteristic behavior of first order phase transitions. (3) The strain peaks at the end of the phase transition, and then decreases slightly as the temperature is held constant. This strain decrease is most likely due to creep of the β-phase under the pressures imposed by the walls of the cylinder. (4) Once the furnace is turned off, a slight decrease in strain is observed due to thermal contraction of the β-phase, followed by (5) a small but sharp drop in strain due to the β to α phase transition. Note that during the β to α phase transition, the temperature of the Pu ingot also increases slightly due to the release of the latent heat of the exothermic β to α phase transition (see Figure 8). (6) Following the β–α phase transition, no further change in the strain is measured indicating that the cylinder was plastically deformed during this cycle.

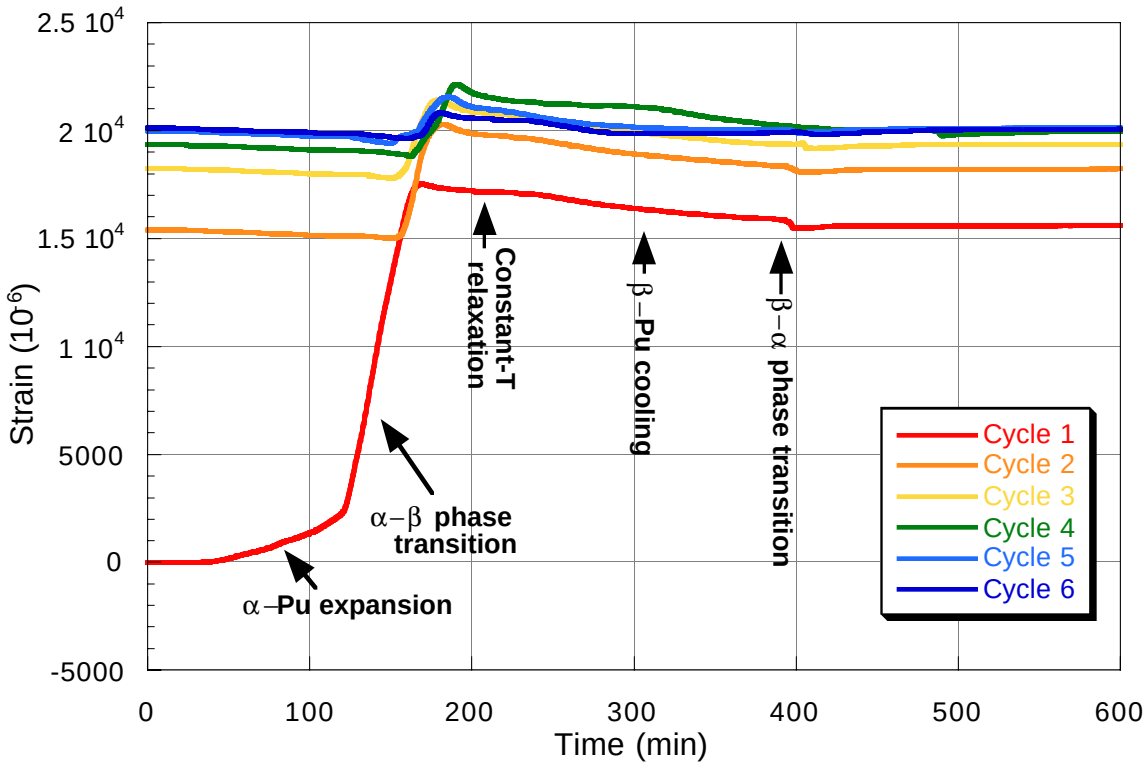

FIG 10
Strain vs. Time response of strain gage #3 for all cycles.

As is evident from Figure 10, most plastic strain in the cylinder is accumulated during the first thermal cycle. With each subsequent cycle, the amount of additional accumulated plastic strain

decreases until cycle 6, in which no additional plastic strain is observed. Plots of the total, plastic, and elastic strain accumulated within each cycle are given in Figure 11 (representing the worst case data from strain gage #3), and Figure 12 (average among all hoop strain gages). The total amount of plastic strain observed for all cycles, obtained by summing the amount of plastic strain accumulated during each cycle, is 1.32% averaged over all hoop strain gages, and the worst case strain is 2.03%, based on strain gage #3.

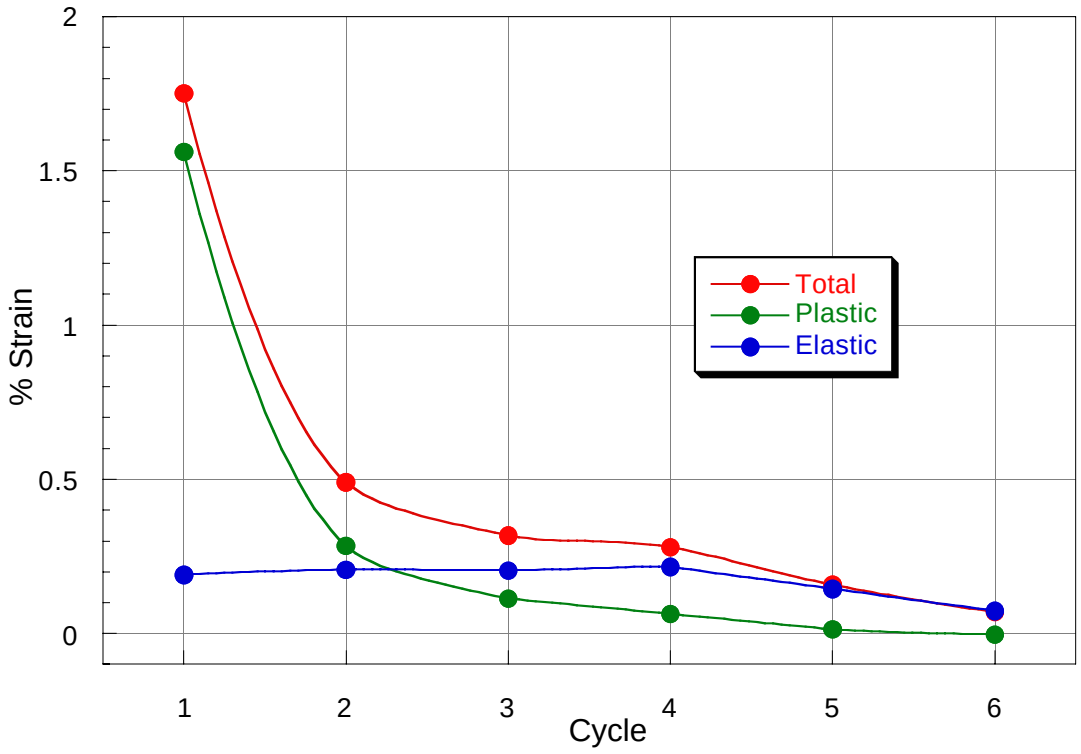

FIG 11

Strain (total, plastic, and elastic) vs. Cycle for strain gage #3.

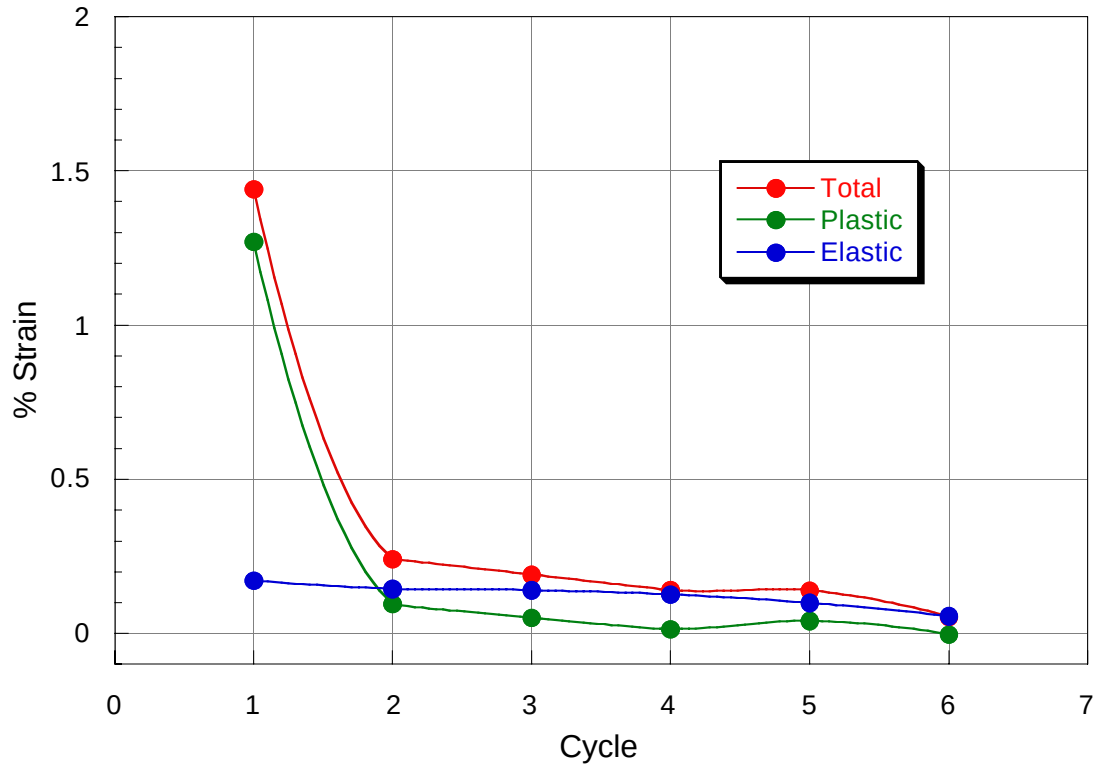

FIG 12

Average Strain vs Cycle.

Dilatometry data is presented for the first and fourth cycle in Figures 13 and 14, respectively. The change in thickness of the ingot was calculated by adding the measurements from the two opposing dilatometers. In Figure 13, both the change in thickness of the ingot and the strain from gage #3 are plotted as a function of temperature. A small increase in thickness (0.001", 0.13%) was observed prior to the onset of the phase transition, which is consistent within error with the linear thermal expansion expected for α-Pu (~0.5%) over the temperature range from ambient to 110°C (Miner and Schonfeld, 1980). Starting at the onset of the phase transition, as indicated by the sharp increase in strain, the thickness increased by 0.042" (5.8%) during heating. This is nearly twice the expected linear thermal expansion (~3%) for the volume expansion associated with the α to β phase transition.

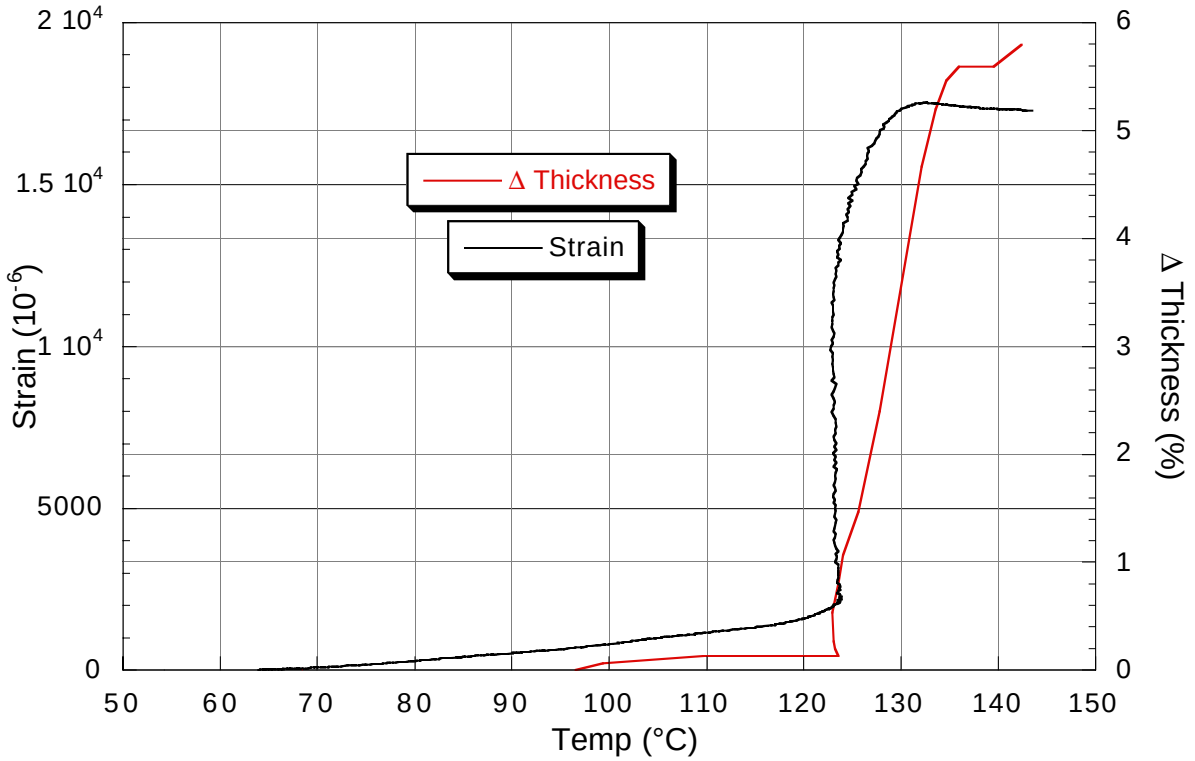

FIG 13

Strain/Thickness vs Temp, first cycle, temp increasing.

In Figure 14, the strain from gage #3 and the thickness change are plotted as a function of time for the fourth cycle. Prior to the onset of the phase transition, a marked *decrease* in thickness (–1.8%) was observed, followed by a modest thickening of the ingot of 0.6% (over the starting thickness) during and after the phase transition.

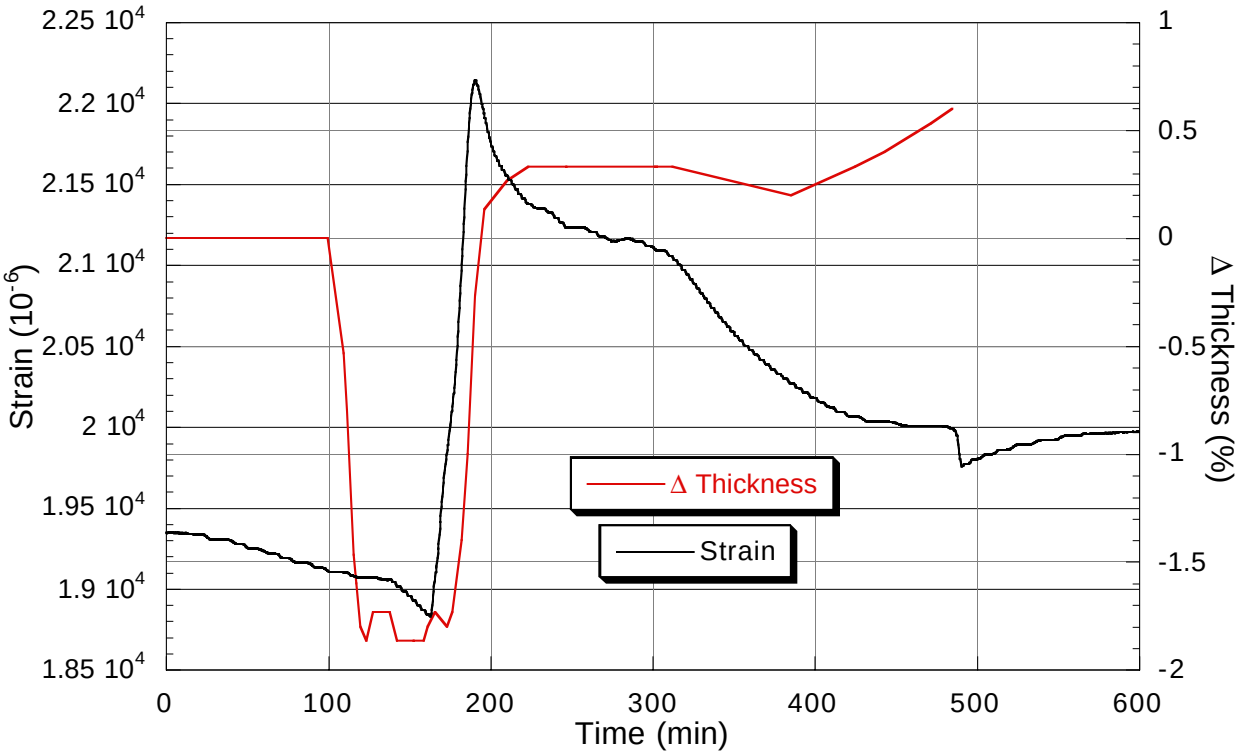

FIG 14

Strain/Thickness vs Time, fourth cycle.

Following the sixth thermal cycle, the ingot was removed from the cylinder and the cylinder outer diameter at the midpoint was measured to have increased by 0.071". Based on an initial OD of 4.477", this represents a 1.58% increase in circumference, in good agreement with the measured strain of 1.32% averaged over all hoop gages. The plastic deformation is visible as a slight bulge in the center of the cylinder, as evident in Figure 15. Despite the low oxygen levels generally maintained in the glovebox (< 30ppm), the Pu ingot showed surface oxidation upon removal from the cylinder (Figure 16). This oxidation may have been a result of above ambient temperatures, and thus higher reactivity, or due to a single overnight loss of negativity in the glovebox which resulted in significantly higher O_2 levels. Despite the coating of oxide, the ingot was still intact as a single massive piece of metal following the experiment with no obvious signs of severe cracking.

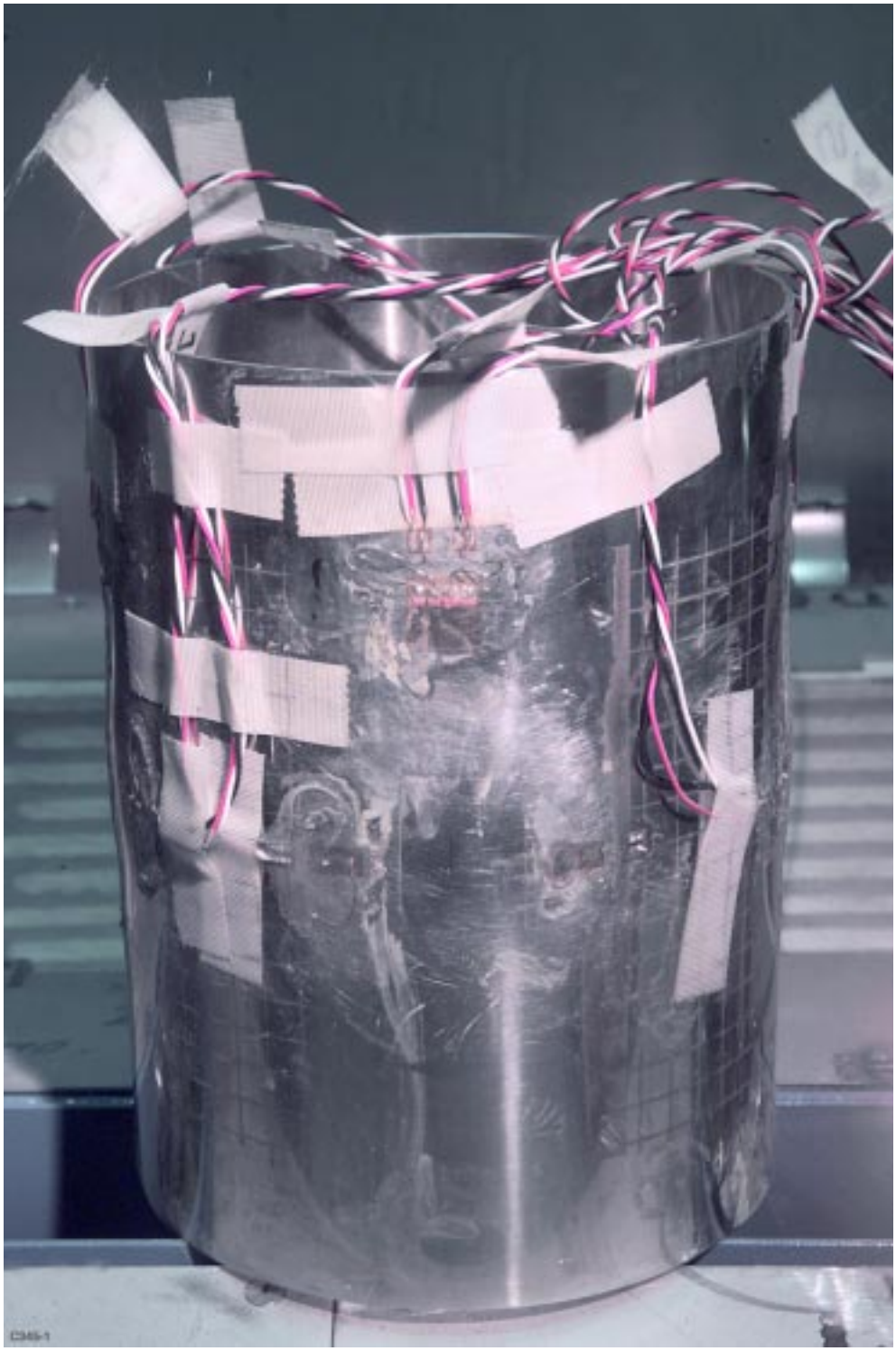

Fig 15 – Cylinder after six thermal cycles. Note plastic deformation around center of cylinder. Cylinder is 6” in length.

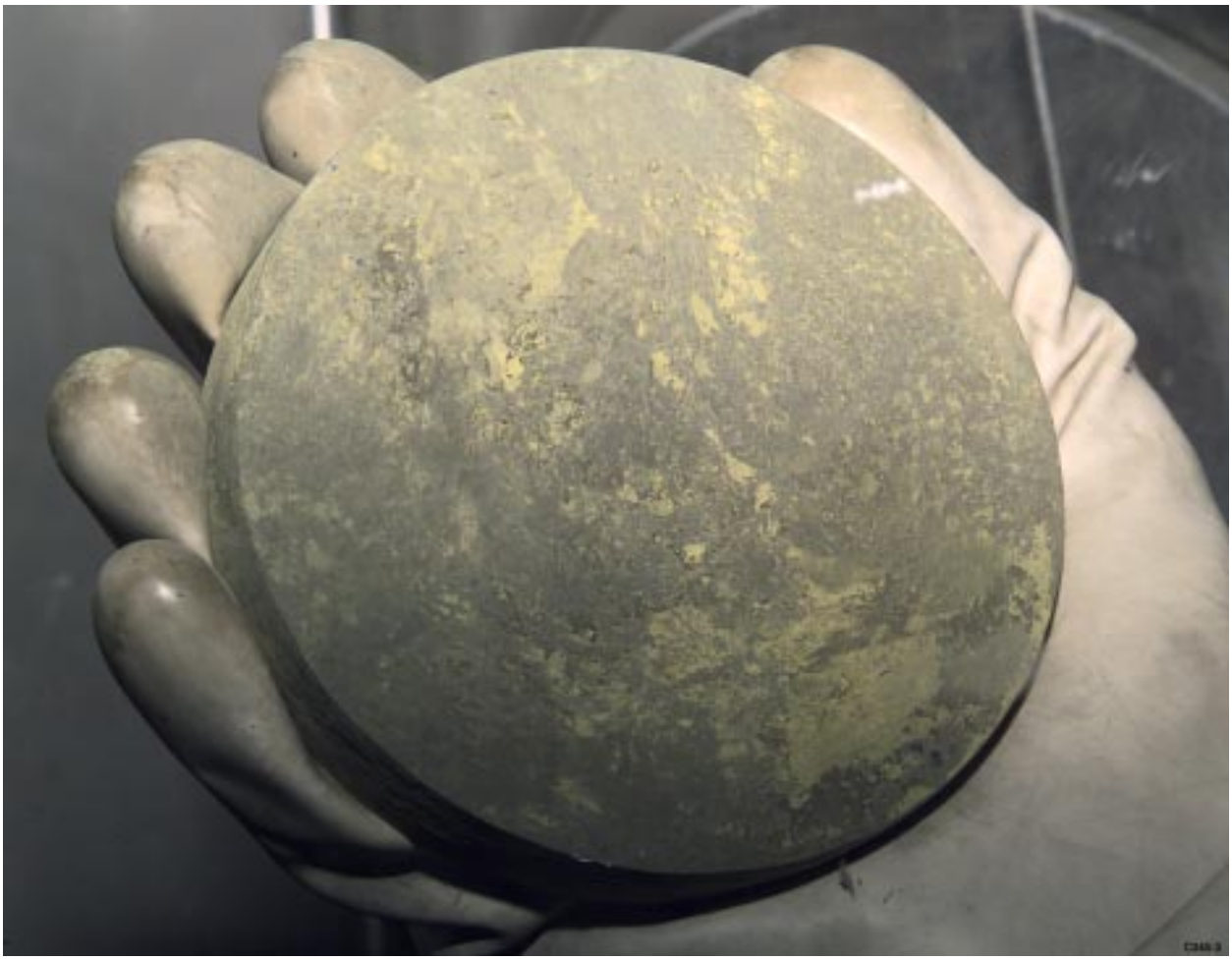

Fig 16 – Pu ingot after six thermal cycles showing moderate surface oxidation.

DISCUSSION

Overall response of the strain gages during thermal cycling is as expected for expansion and contraction of the Pu ingot within the stainless steel cylinder. The hoop strain gages all showed positive strains, while the longitudinal gages showed a slight negative strain, corresponding to compression, which is consistent with radial expansion of the cylinder. The results from this experiment also are consistent with what was observed in the previous experiment, with several notable exceptions. In both the previous experiment and the one reported herein, no additional plastic strain was incurred after the fifth thermal cycle, and the ingot was observed to have thickened more than would be expected based on isotropic volume expansion during the phase

transition. In contrast, the total amount of plastic strain observed in the previous experiment was 0.2%, compared with 1.32% for the current experiment. This difference can be attributed to the differences in the canisters used. The previous experiment utilized a work-hardened canister, while a fully annealed canister was used for the current experiment. As would be expected, the work-hardened canister from the previous experiment also showed higher elastic strain levels (0.5%) relative to the annealed canister in this experiment (0.2-0.3%). This result also is consistent with the observation that there was a larger change in the thickness of the ingot in the previous experiment (~10%) relative to the current experiment (5.6%). The work-hardened can was stronger (120,000 psi yield strength) than the fully annealed can (40,600 psi yield strength), and was thus able to "push back" on the ingot creating higher radial compressive stresses.

Based on the mechanics of thin-walled cylinders, the radial compressive stresses experienced by the Pu ingot during the phase transition can be estimated based on the following relationship:

$$\sigma = \frac{Pr}{t}$$

Where σ = wall stress, P = internal pressure, r = radius of cylinder, and t = wall thickness. As a simple approximation, the wall stress can be set equal to the tension yield strength of stainless steel. The tension yield strength for the cylinder used in this experiment (as measured by Savannah River) is 40,600 psi. Using the appropriate dimensions of the cylinder (r = 2.181", t = 0.060"), the calculated internal pressure, equivalent to the compressive stress applied to the Pu ingot, as a result of the expansion is 1117 psi.

The radial compressive stress on the ingot also can be calculated using the measured strain values from this experiment. Recall that $\sigma=E\varepsilon$, where E = Young's Modulus and ε = strain. Thus, substituting $E\varepsilon$ for stress in the above equation and solving for P:

$$P = \frac{E\varepsilon t}{r}$$

Using the elastic strain value of 0.00171 (0.171%) from the first cycle, and a Young's Modulus of 27.3e6, as measured by SRS for this steel at the α to β transition temperature, the calculated radial pressure on the ingot due to the cylinder walls is 1284 psi. These values are in excellent agreement,

considering that the calculation based on the actual observed elastic strain value will slightly overestimate the actual pressure. This over-estimation is due to the inherent assumption that all of the elastic strain is creating back pressure on the ingot, and that no simultaneous plastic deformation occurrs.

The calculated values of radial compressive stress imparted on the Pu ingot by the cylinder wall are far less than the compressive yield strength values of both α-Pu (~60,000 psi) and β-Pu (~20,000 psi) at the transition temperature (Miner and Schonfeld, 1980). Therefore, the axial deformation observed in the Pu ingot must be due to some mechanism other than simple compressive yield. This is consistent with previous observations that stresses applied during either the α to β or β to α phase transitions produce pronounced cyrstallographic and microstructural shape texturing (Elliot et al., 1964; Spriet, 1965). Thus, during recrystallization, a preferential grain alignment is established perpendicular to the radial stresses imposed by the walls of the cylinder, resulting in a thickening of the ingot greater than would be expected based on isotropic expansion. The greatest amount of strain would therefore be placed on the cylinder during the first cycle when the grain orientation is random. Additional cylinder strain from subsequent cycles would be substantially less due to the preferred grain alignment perpendicular to the stress direction and accompanying preferred expansion in the axial direction, which is exactly what is observed in the experimental strain data.

The equilibrium temperature for the α to β phase transition is 120°C (Stephens, 1963). However, in all cycles the observed onset of the α to β phase transition was around 123°C and the onset of the β to α back transformation was around 75°C. These values are consistent with the known T-T-T behavior of Pu (Nelson, 1967; Nelson, 1980). The α–β start time is quite long (> 1000s) at temperatures below about 120°C. At 140°C, the maximum temperature that the ingot reached during the thermal cycling, the α to β completion time in on the order of 10^3 seconds, which is consistent with what was observed. For the β to α back transformation, the T-T-T curves show that the transformation times do not reach values of less than 10^3 seconds until the

temperature is less than about 80°C, which is also consistent with what was observed in the current experiment.

The increase in ingot thickness though the phase transition for the first cycle, as depicted in Figure 13, is expected. As mentioned above, the increase in thickness beyond the amount anticipated for isotropic expansion is due to preferential grain alignment during recrystallization as a result of the imposed stresses from the cylinder wall. The decrease in ingot thickness observed immediately prior to the α to β phase transition (Figure 14) for all cycles following the first could be the result of two different factors. One possibility is that some β-Pu is retained upon cooling from the previous cycle. During the heating phase of the next cycle, this quenched β-Pu recrystallizes prior to the phase transition. However, this seems an unlikely possibility as the β to α T-T-T curves show that the β to α transformation is most efficient between –40 and +40°C (Nelson, 1967). Even at 50°C (the equilibrium temperature of the Pu ingot in this experiment), the transition begins in less than 10 seconds, and is 5% complete in only 12 seconds. A more likely explanation of the contraction of the ingot immediately prior to the α to β phase transition is annealing of microcracks formed in the α-Pu as a result of the previous β to α transformation. As has been previously reported (Nelson, 1966), the volume expansion associated with cycling Pu across the α/β phase transition is due to the formation of microcracks. The microcracks can be annealed out by heating α -Pu to within 10-20°C of the transition temperature (Huang and Jenkins, 1998). Thus, it seems more likely that the contraction observed prior to the onset of the phase transition is due to the annealing of microcracks within α-Pu than recrystallization of residual β-Pu back to α-Pu. Regardless of the mechanism, the observed contraction appears to have little effect on the overall integrity or deformation of the cylinder.

It is readily apparent from Figures 8 and 9 that not all strain gages showed response to the phase transition at exactly the same time (or temperature, relative to the ingot temperature), nor do they show the same values of total strain. This result may in part be due to non-uniform expansion of the ingot or slight asymmetry in the roundness of the cylinder or ingot causing the ingot to come in contact with different parts of the cylinder wall at different times. However, a more likely

explanation is differential heating effects and temperature inhomogeneity. The cylinder and ingot in this experiment were not in the radial center of the furnace, thereby resulting in differential heating. A plot of the temperature recorded by the three thermocouples on the outside of the cylinder as a function of the thermocouple on the Pu ingot inside the cylinder upon heating between ambient and 115°C upon heating (i.e. - prior to temperature effects induced by the phase transition) is given in Figure 17.

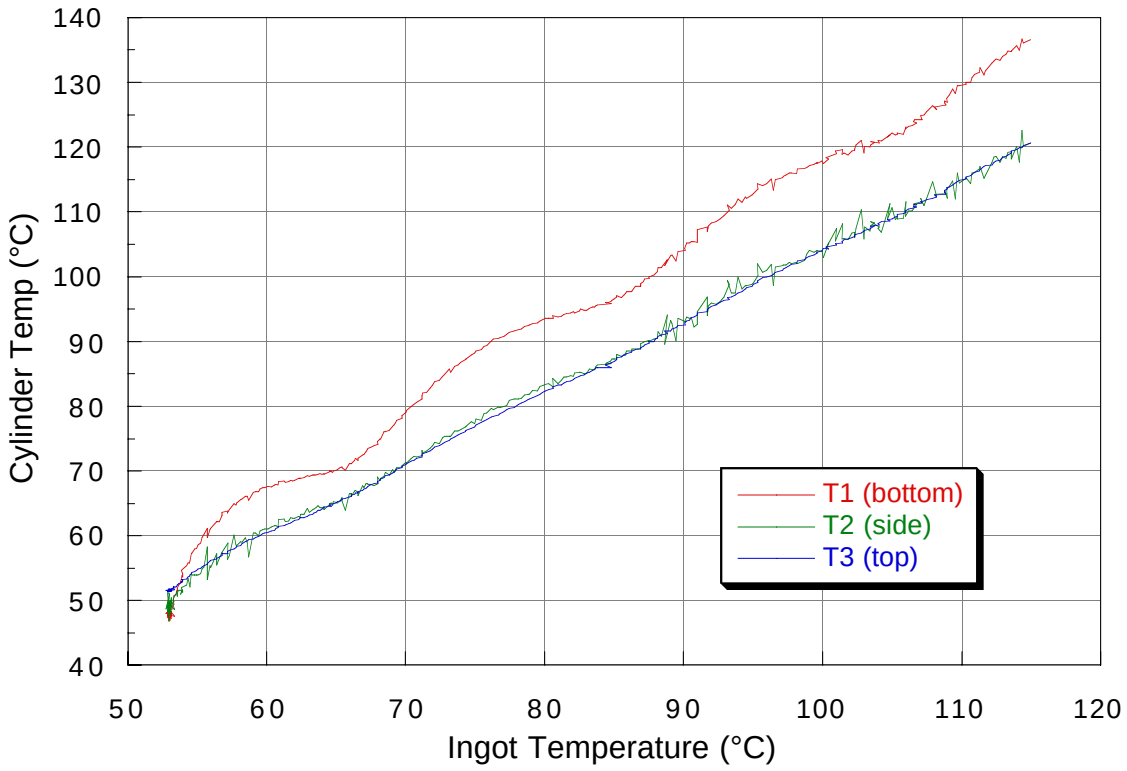

FIG 17

Cylinder temperatures vs. ingot temperature.

The ingot temperature was used as the independent variable in this case due to the thermal stability that the large mass of Pu presents, and thus is not affected severely by minor temperature fluctuations and gradients in the furnace environment. The thermocouple on the bottom of the cylinder (T1), nearest to the heating elements of the furnace, consistently shows a higher temperature than the thermocouple on the side and top of the can, relative to the ingot temperature.

The furnace controller induced fluctuations are also readily apparent in the output from T1. The bottom of the cylinder, and presumably the bottom of the ingot, were therefore consistently hotter than the remainder of the cylinder. Thus, the bottom of the ingot transformed earlier in time than the top. Non-uniform heating actually results in a more severe test of the canister integrity than uniform heating due to a non-uniform stress distribution which accentuates the strain at the top of the can. Non-uniform heating also represents a more realistic scenario than does completely uniform heating with respect to canister integrity by producing localized high-strain areas.

CONCLUSION

Based on the experimental results detailed herein, the highest level of total plastic strain that was imparted on the stainless steel cylinder by the Pu ingot was 2.03%, based on strain gage #3. If the ~0.2% elastic strain is added to this, then the total amount of strain (plastic plus elastic) experienced by the cylinder was ~2.2%. However, the average total plastic strain, based on all hoop strain gages, is only 1.32%. These strain levels are far below the plastic failure strain levels for this type of stainless steel. Using the measured elastic strain values, the maximum radial compressive stress that the cylinder could impart upon the Pu ingot is about 1,300 psi (and is most likely considerably less). The result of this compressive stress is that expansion of the ingot in the axial direction was measured to be greater than 5%, which is well above the 3% expected for isotropic expansion. This enhanced axial expansion is attributed to preferential grain orientation of the β-Pu along the axial direction (perpendicular to the stress direction).

Repeated thermal cycling of the ingot resulted in a decrease in the amount of additional plastic strain accumulated within each cycle, such that by cycle 6 no additional plastic strain was imparted upon the cylinder. This decrease is attributed to a combination of the preferential orientation of grain growth during the α/β phase transition, thereby limiting the expansion in the radial direction, and a saturation of the total volume expansion associated with thermal cycling of the Pu through the phase transition. Based on the experimental evidence presented herein, failure of a DOE standard 3013 storage canister due solely to strain imparted on it by expansion associated with

thermal cycling of Pu through the α/β phase transition stored within does not appear to be credible. Finite Element Analysis modeling by Savannah River will further analyze these findings.

ACKNOWLEDGEMENTS

The authors would like to thank Arthur “Lonny” Morgan and Ann Schake for their invaluable assistance in setting up and conducting this study. We are also greatly indebted to the following LANL Plutonium Foundry personnel for their outstanding efforts in casting and machining the plutonium ingot used in this experiment: John Huang, Charles Puglisi, Kenny Vigil, Anthony Valdez, Floyd Rodriguez, Theresa Abeyta, Steve Boggs, and Pat Rodriguez.
This work was supported by the Nuclear Materials Stewardship Project Office of the United States Department of Energy.

REFERENCES CITED

ASME (1995) Section VIII, Division 2. Boiler and Pressure Vessel Code. American Society of Mechanical Engineers.

DOE (1996). Criteria for preparing and packaging plutonium metals and oxides for long-term storage. DOE-STD-3013-96. US Department of Energy.

Elliot, R.O., Olsen, C.E., and Bronisz, S.E. (1964) Effect of preferred orientation on the electrical resistivity of alpha plutonium at low temperatures. Physical Review Letters, 12, 276-278.

Flamm, B.F., Prenger, F.C., Veirs, D.K., Hill, D.D., and Isom, G.M. (1997). Effects on the long term storage container by thermal cycling alpha plutonium. LA-UR-97-4439. Los Alamos National Laboratory

Gardner, H.R. (1980) Mechanical Properties. In O. J. Wick (eds), Plutonium Handbook, p. 59-100. The American Nuclear Society, La Grange Park, IL.

Huang, J., and Jenkins, T. (1998). Annealing of α-Pu. Personal Communication. Los Alamos National Laboratory.

Miner, W.N., and Schonfeld, F.W. (1980) Physical Properties. In O. J. Wick (eds), Plutonium Handbook, p. 31-57. American Nuclear Society, La Grange Park, IL.

Nelson, R.D. (1966) Phase transformation damage in plutonium. Journal of Nuclear Materials, 20, 153-161.

Nelson, R.D. (1967) The plutonium β–α TTT curve. Journal of Nuclear Materials, 23, 238-240.

Nelson, R.D. (1980) Solid State Reactions. In O. J. Wick (eds), Plutonium Handbook, p. 101-143. American Nuclear Society, La Grange Park, IL.

Nelson, R.D., and Shyne, J.C. (1966a) Characteristics of beta-alpha and alpha-beta tranformations in plutonium. Transactions of the Metallurgical Society of AIME, 236, 1725-1731.

Nelson, R.D., and Shyne, J.C. (1966b) Comments on kinetics of the α–β and β–α transformations of plutonium in e vicinity of equilibrium. Journal of Nuclear Materials, 19, 345-347.

Rechtien, J.J., and Nelson, R.D. (1973) Phase transformations in uranium, plutonium, and neptunium. Metallurgical Transactions, 4, 2755-2765.

Spriet, B. (1965). Study of allotropic transformation of plutonium. In A. E. Kay & M. B. Waldron (Ed.), Plutonium 1965, (pp. 88-?). London: Chapman and Hall for The Institute of Metals

Stephens, D.R. (1963) The phase diagram of plutonium. Journal of Physics and Chemistry of Solids, 24, 1197-1202.